Archives of Acoustics Vol. 46, No. 4, pp. 591–604 (2021), doi: 10.24425/aoa.2021.138152

Research Paper

Numerical Model of Surface and Quasi-Spherical Sea Noise and Its Application to Analysis of DIFAR Systems

Mariusz RUDNICKI*, Roman SALAMON, Jacek MARSZAL

Gdansk University of Technology, Faculty of Electronics, Telecommunications and Informatics
Department of Sonar Systems
Gdansk, Poland
*Corresponding Author e-mail: mariusz.rudnicki@pg.edu.pl

(*received April 26, 2021; accepted August 31, 2021*)

Various types of passive sonar systems are used to detect submarines. These activities are complex and demanding. Therefore, computer simulations are most often used at the design stage of these systems. For this reason, it is also necessary to simulate the acoustic ambient noise of the sea. The article proposes a new numerical model of surface and quasi-spherical sea noise and presents its statistical parameters. The results of the application of the developed noise model to analyse the received signals of the DIFAR[1] sonobuoy are also presented.

Keywords: numerical model; surface and quasi-spherical sea noise; DIFAR; bearing errors.

1. Introduction

In active and passive sonar systems, the signal-to-noise ratio at the receiver input determines the range and accuracy of bearings of the objects observed. The acoustic ambient noise of the water medium in which the system operates is often the predominant noise. It can be shown that, in addition to the noise level, the range and accuracy of bearings also depend on noise correlation (Rudnicki *et al.*, 2020). The problem also applies to detection in underwater acoustic communications UAC (Kochańska *et al.*, 2018; Schmidt *et al.*, 2018). Active, narrow-band systems typically assume that acoustic ambient noise is uncorrelated (Burdick, 1984; Urick, 1983; 1986). In active systems, the distance between adjacent antenna elements is typically about half the wavelength of the sonar operating frequency. In passive systems of the DIFAR type, this condition is not met because the distance between the hydrophones placed in the antenna is always much smaller than the length of the waves of the received signals.

At the present moment, a major and commonly used method of system design is computer simulation, with the use of tools such as MATLAB®. It requires the development of a numerical model for the received signal and noise. The reliability of the simulation results depends on the similarity of the numerical versions of the signal and noise to their real analogue nature present in the environment. Rudnicki *et al.*, (2020) present a developed numerical model of isotropic sea noise and use it to analyse bearing errors in the DIFAR system. They have extended this model to include surface noise caused by waving, dominating in low frequencies (it does not take into account the noise associated with human activity, emitted by ships, coastal industry, living organisms, etc.) (Ren, Huang, 2020; Klusek, Lisimenka, 2016; Kozaczka, Grelowska, 2011; Grelowska *et al.*, 2013).

The numerical model of such noise presented below was designed to achieve similarity of their correlation functions to those determined in theory and experimentally.

[1]Directional Frequency Analysis and Recording (DIFAR) is the most widely used sonobuoys system for the detection and location of submarines. It is a passive system containing five hydrophones that form the crossed two pairs of gradient hydrophones and an additional central hydrophone (Mallet, 1975; Salamon, 2004; Rudnicki *et al.*, 2020).

2. Numerical model of surface noise

Surface sea noise is emitted in the waving process and its level depends on the sea state. It is mainly in the frequency range up to several dozen kilohertz, and its level decreases at a rate of about 6 dB/octave (Burdick, 1984; Urick, 1983; 1986; Klusek, Lisimenka, 2016). To put it simply, the surface sea noise emission mechanism is based on the collapse of air bubbles sucked into the sea by waves, especially waves that break in high wind (Klusek, Lisimenka, 2004). Collapsing air bubbles generate acoustic pulses whose narrow band spectrum is similar to the Gaussian noise spectrum. Based on these properties of the sea wave noise, it was assumed that the sources of surface noise are points emitting acoustic waves with a time course described by white Gaussian noise. Two types of sources were initially considered, namely, single spherical wave sources and double dipole sources having a directional radiation pattern similar to that in Fig. 8 (Crocker, 1998). The motivation for using dipole sources was brought about by the conditions for acoustic wave reflection at the water-air boundary. As it is known, an acoustic wave in water is the superposition of a wave emitted by a spherical source located below the water surface and by a virtual spherical source in the air. The virtual source is symmetrical in relation to the real source and emits a wave with a sign opposite to the wave generated by the real source (Crocker, 1998).

The following are the geometric relationships for the model with dipole sources. The analysis was performed for a receiving antenna consisting of 7 non-directional hydrophones. Five of them, located in the horizontal plane (H_0, H_1, H_2, H_3, and H_4), form a configuration analogous to that in the DIFAR type system, and two additional ones (H_5 and H_6) complete the configuration of the antenna in the vertical direction. It is assumed that K of the dipole sources is distributed randomly but statistically evenly in a circle with a radius of R with a surface density of ρ. The centre of the circle is on the surface of the water and on a straight line passing through the vertically located antenna hydrophones (H_5, H_0, and H_6), as shown in Fig. 1. The centre of the X, Y, Z spatial system under consideration is the central hydrophone H_0 of the antenna. The XY plane is parallel to the sea surface and the centre of the antenna is immersed at a depth of h. It is assumed that each point noise source emits a spherical wave of equal intensity.

In order to determine the correlation function of the noise received by the pair of hydrophones lying on the coordinate axes, one must calculate the distances between the individual point sources of noise and the hydrophones of the antenna. Because the spatial system under consideration is symmetrical in relation to the Z-axis, the formulas presented will be limited to the analysis of the noise received by the two horizontal hydrophones in the horizontal plane (marked by indexes 1 and 2) and by two in the Z-axis (marked by indexes 5 and 6).

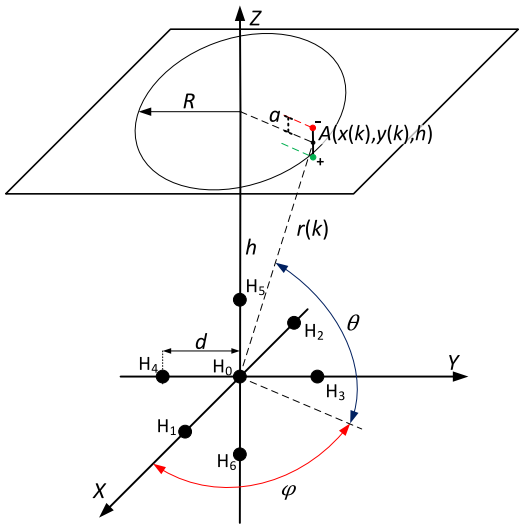

Fig. 1. Geometry of the sea wave noise model.

The distances of the k-dipole source from the hydrophones are equal to:

$$r(k) = \sqrt{x^2(k) + y^2(k) + h^2}, \tag{1}$$

$$r_{1-}(k) = \sqrt{[x(k) - d]^2 + y^2(k) + (h + a)^2}, \tag{2}$$

$$r_{1+}(k) = \sqrt{[x\,(k) - d]^2 + y^2\,(k) + (h - a)^2}, \tag{3}$$

$$r_{2-}(k) = \sqrt{[x\,(k) + d]^2 + y^2\,(k) + (h + a)^2}, \tag{4}$$

$$r_{2+}(k) = \sqrt{[x\,(k) + d]^2 + y^2\,(k) + (h - a)^2}, \tag{5}$$

$$r_{5-}(k) = \sqrt{x(k)^2 + y^2\,(k) + (h - d + a)^2}, \tag{6}$$

$$r_{5+}(k) = \sqrt{x(k)^2 + y^2\,(k) + (h - d - a)^2}, \tag{7}$$

$$r_{6-}(k) = \sqrt{x(k)^2 + y^2\,(k) + (h + d + a)^2}, \tag{8}$$

$$r_{6+}(k) = \sqrt{x(k)^2 + y^2\,(k) + (h + d - a)^2}, \tag{9}$$

where $r(k)$ is the distance from the centre of the k-dipole to the centre of the antenna, the sign "–" indicates the distance from the virtual source and the sign "+" from the real source, d determines the distance from hydrophones H_1, ..., H_6 to the central hydrophone H_0, and a indicates the distance from real or virtual source to the centre of the k-dipole.

The times of wave propagation from the sources to the hydrophones are:

$$\tau(k) = \frac{r(k)}{c}, \qquad \tau_{i-}(k) = \frac{r_{i-}(k)}{c}, \qquad \tau_{i+}(k) = \frac{r_{i+}(k)}{c}, \tag{10}$$

where c is the acoustic wave speed in water, and the i index is the hydrophone number.

Using formulas (1)–(9) and assuming that $r_i(k) \approx r(k)$ and $a \ll h$ and $d \ll h$, the following are obtained approximately for all hydrophones:

$$\tau_{1-}(k) - \tau(k) \cong \frac{-dx(k) + ha}{cr(k)}, \qquad \tau_{1+}(k) - \tau(k) \cong \frac{-dx(k) - ha}{cr(k)}, \tag{11}$$

$$\tau_{2-}(k) - \tau(k) \cong \frac{dx(k) + ha}{cr(k)}, \qquad \tau_{2+}(k) - \tau(k) \cong \frac{dx(k) - ha}{cr(k)}, \tag{12}$$

$$\tau_{5-}(k) - \tau(k) \cong \frac{-h(d-a)}{cr(k)}, \qquad \tau_{5+}(k) - \tau(k) \cong \frac{-h(d+a)}{cr(k)}, \tag{13}$$

$$\tau_{6-}(k) - \tau(k) \cong \frac{h(d+a)}{cr(k)}, \qquad \tau_{6+}(k) - \tau(k) \cong \frac{h(d-a)}{cr(k)}. \tag{14}$$

Let us now introduce the following symbols:

$$\tau_x(k) \cong \frac{dx(k)}{cr(k)}, \quad \tau_d(k) \cong \frac{hd}{cr(k)}, \quad \tau_a(k) \cong \frac{ha}{cr(k)}. \tag{15}$$

For such symbols, the dependencies (11)–(14) can be expressed as:

$$\tau_{1-}(k) = -\tau_x(k) + \tau_a(k) + \tau(k), \qquad \tau_{1+}(k) = -\tau_x(k) - \tau_a(k) + \tau(k), \tag{16}$$

$$\tau_{2-}(k) = \tau_x(k) + \tau_a(k) + \tau(k), \qquad \tau_{2+}(k) = \tau_x(k) - \tau_a(k) + \tau(k), \tag{17}$$

$$\tau_{5-}(k) = -\tau_d(k) + \tau_a(k) + \tau(k), \qquad \tau_{5+}(k) = -\tau_d(k) - \tau_a(k) + \tau(k), \tag{18}$$

$$\tau_{6-}(k) = \tau_d(k) + \tau_a(k) + \tau(k), \qquad \tau_{6+}(k) = \tau_d(k) - \tau_a(k) + \tau(k). \tag{19}$$

Figures 2 and 3 illustrate the correctness of the simplifications used. Figure 2 shows the delays calculated from formulas (1)–(3) and from the simplified formulas (15). Figure 3 presents the differences in the delays shown in Fig. 2. As one can see, the differences in delays are small and are mainly due to time discretisation in formulas (1)–(3). The sampling rate is marked as f_s, and the duration of one measurement cycle is T.

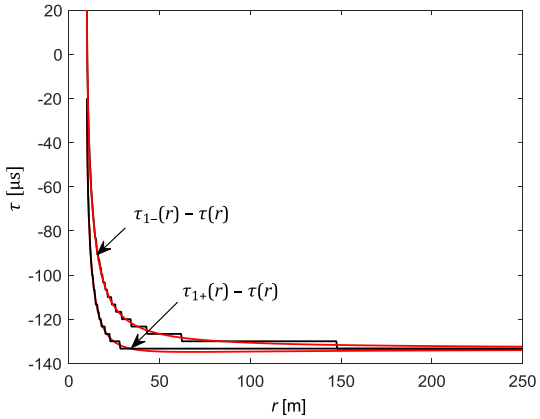

Fig. 2. Delays of the noise received by the hydrophones; red line – from formulas (15), black line – from formulas (1)–(3) (R = 250 m, h = 10 m, K = 500, d = 0.2 m, a = 0.03 m, f_s = 0.3 MHz, T = 0.1 s).

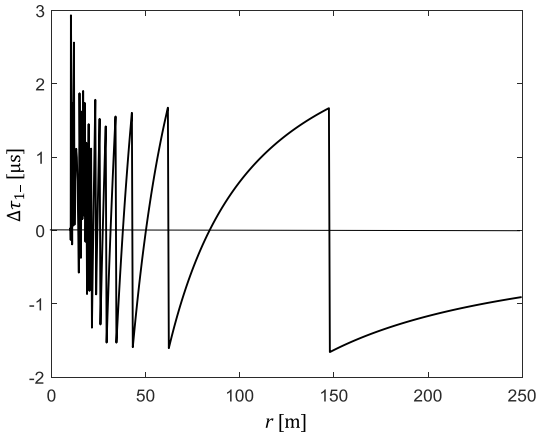

Fig. 3. Difference in the delays calculated from formulas (1)–(3) and formulas (15) (parameters as in Fig. 2).

The $n_i(t)$ noise received by the i-th hydrophone[2] is the difference of the noise from the real and virtual sources. Assuming a spherical propagation model, there is:

$$n_i(t,k) = \frac{r_0}{r(k)} \left\{ n\left[t - \tau_{i-}(k)\right] - n\left[t - \tau_{i+}(k)\right] \right\}, \tag{20}$$

where r_0 is the unit distance.

[2]The numerical value of the voltage at the hydrophone output is proportional to the sound pressure of sea noise. The purpose of the simulation is to test the correlation properties of noise, and therefore the use of any unit of measurement may be neglected.

In order to evaluate the amount of noise received by each hydrophone, we determine the Fourier transform of Eq. (20). It is as follows:

$$N_i(j\omega,k) = \frac{r_0}{r(k)}\left[e^{j\omega\tau_{i-}(k)} - e^{j\omega\tau_{i+}(k)}\right]N(j\omega,k), \quad (21)$$

where $N(j\omega,k) = \Im\{n(t,k)\}$.

Using dependencies (11)–(14), we obtain the spectra of noise received by each hydrophone:

$$N_1(j\omega,k) = \frac{r_0}{r(k)}e^{j\omega[\tau(k)-\tau_x(k)]} \cdot\left[e^{j\omega\tau_a(k)} - e^{-j\omega\tau_a(k)}\right]N(j\omega,k), \quad (22)$$

$$N_2(j\omega,k) = \frac{r_0}{r(k)}e^{j\omega[\tau(k)+\tau_x(k)]} \cdot\left[e^{j\omega\tau_a(k)} - e^{-j\omega\tau_a(k)}\right]N(j\omega,k), \quad (23)$$

$$N_5(j\omega,k) = \frac{r_0}{r(k)}e^{j\omega[\tau(k)-\tau_d(k)]} \cdot\left[e^{j\omega\tau_a(k)} - e^{-j\omega\tau_a(k)}\right]N(j\omega,k), \quad (24)$$

$$N_6(j\omega,k) = \frac{r_0}{r(k)}e^{j\omega[\tau(k)+\tau_d(k)]} \cdot\left[e^{j\omega\tau_a(k)} - e^{-j\omega\tau_a(k)}\right]N(j\omega,k). \quad (25)$$

Expressions before the square brackets describe shifts of the phase of noise received and do not affect the amount of noise. The determining factor of the amount of noise received is the same in formulas (22)–(25) and is as follows:

$$A(j\omega,k) = \frac{2jr_0}{r(k)}\sin\left[\omega\tau_a(k)\right]N(j\omega,k). \quad (26)$$

Replacing τ_a with the expression from formula (15) results in the following:

$$A(j\omega,k) = \frac{2jr_0}{r(k)}\sin\left[\omega\frac{ah}{cr(k)}\right]N(j\omega,k). \quad (27)$$

In order to simplify the model, we assume that the argument of the sine function takes small values and then it can be replaced by its argument. Assuming that the limit value of the argument is $\pi/6$, the following simplification condition is obtained:

$$\omega\frac{ah}{cr(k)} < \frac{\pi}{6}. \quad (28)$$

The upper frequency f_g of the noise spectrum occurs at the minimum distance $r(k) = h$ and is:

$$f_g = \frac{c}{12a}. \quad (29)$$

In the frequency range $f < f_g$, formula (27) can be expressed as:

$$A(j\omega,k) \cong \frac{2jr_0}{r(k)}\frac{\omega ah}{cr(k)}N(j\omega,k). \quad (30)$$

At a constant noise power spectral density $a(t,k) = \Im^{-1}\{A(j\omega,k)\}$ the amount of noise is proportional to the noise derivative $n(t,k)$.

If we assume that the noise pressure spectrum decreases at a rate of −6 dB/oct of the frequency beginning with a certain frequency of ω_0, then the spectrum $N(j\omega,k)$ can be expressed as $N(j\omega,k) = (\omega_0/\omega)N_0(j\omega,k)$, where $N_0(j\omega,k)$ is the spectrum of Gaussian noise. The result is:

$$A(j\omega,k) = \frac{2jr_0}{r^2(k)}\frac{\omega_0 ah}{c}N_0(j\omega,k) \quad \text{for} \quad \omega > \omega_0. \quad (31)$$

After the determination of the inverse Fourier transform, we obtain a description of the noise received by the hydrophones:

$$a(t,k) = \frac{2jr_0}{r^2(k)}\frac{\omega_0 ah}{c}n(t,k) \quad \text{for} \quad \omega > \omega_0. \quad (32)$$

Excluding the delay of $\tau(k)$ in formulas (22)–(25), after determining the inverse Fourier transform, we obtain the following noise time-domain expression:

$$n_1(t,k) = a[t+\tau_x(k),k], \quad (33)$$

$$n_2(t,k) = a[t-\tau_x(k),k], \quad (34)$$

$$n_5(t,k) = a[t+\tau_d(k),k], \quad (35)$$

$$n_6(t,k) = a[t-\tau_d(k),k]. \quad (36)$$

The noise emitted by all K sources is summed, resulting in:

$$n_{si}(t) = \sum_{k=1}^{K} n_i(t,k), \qquad i = 1,2,5,6. \quad (37)$$

The conversions made above led to a significant simplification of the numerical procedure for determining the noise received by the hydrophones. In a non-simplified version of the model, it is necessary to determine the distances from the virtual sources to the hydrophones from formulas (2)–(9) and the corresponding delays of noise received from these distances. In the simplified model, the delays are calculated using formulas (15) which only requires the calculation of the distance $r(k)$ from formula (1). As a result, the number of numerical operations decreases twelvefold, which is important in the case of a very large number of noise samples processed in the model. In addition, there are no limits to the noise bandwidth, since any small values of a can be used in formula (29) without compromising the accuracy of the calculations.

The correctness of the simplifications made has been verified by establishing the dependency of the standard deviation of noise received by the hydrophones from their distance r to the sources of noise. According to formula (30), the standard deviation should be inversely proportional to the distance when excluding the impact of propagation. The sample result of such verification shown in Fig. 4 and other calculations fully confirm the validity of the conversions carried out.

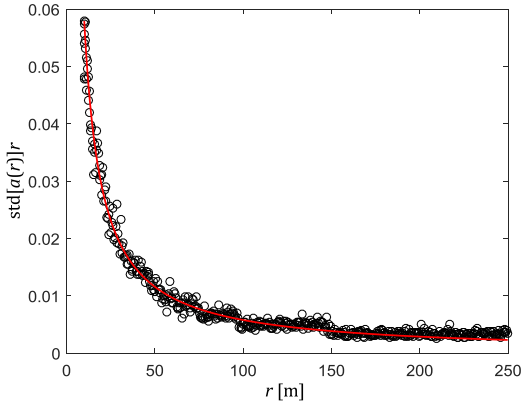

Fig. 4. Standard deviation of noise as a function source distance (∘ – from formula (19), red line – from formula (32), $R = 250$ m, $h = 10$ m, $K = 500$, $d = 0.2$ m, $a = 0.03$ m).

It follows from formula (30) that the module of spectrum of noise received by the hydrophones should grow linearly as a function of frequency. Figure 5 shows an example of a spectrum module and a designated trend line for the source of white Gaussian noise.

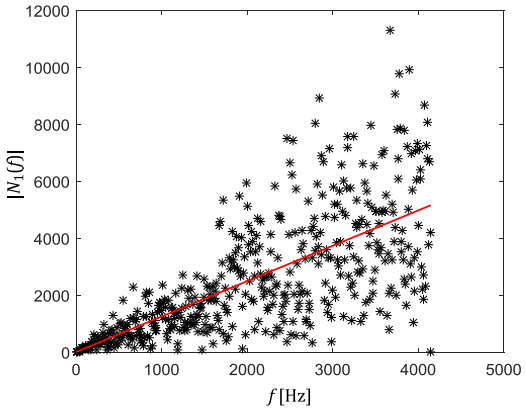

Fig. 5. Module of the spectrum of noise received by the hydrophone (⋆ from formula (21), red line – trend line; parameters as in Fig. 4).

Assuming, according to the results of the measurements of noise spectral density presented in the literature (Burdick, 1984; Urick, 1983; 1986; Salamon, 2006), that in the range of approximately 500 Hz to several dozen kilohertz, it decreases at a rate of 6 dB/oct of frequency, the noise spectrum was multiplied by the function marked with the red line in Fig. 6.

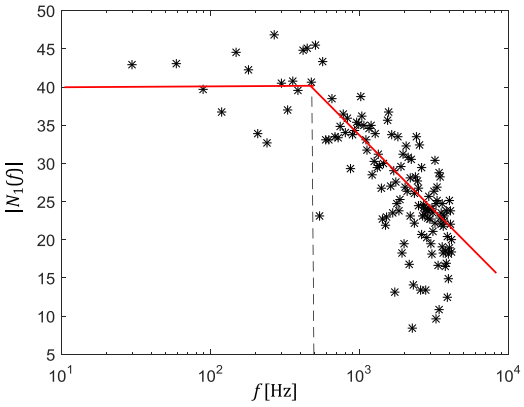

Fig. 6. Spectrum module of noise with a decreasing spectral density of 20 dB/dec (parameters as in Fig. 4).

As a result, the module of noise emitted by the sources has changed as shown in this figure. This change results in the course of the spectrum module of noise received by the hydrophone shown in Fig. 7. According to formula (31), the average value of the module as shown by the trend line is virtually constant.

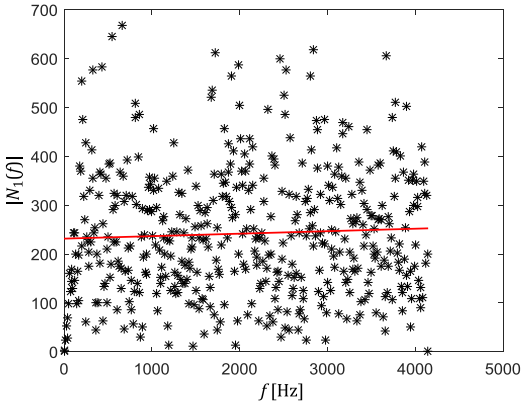

Fig. 7. Module of the spectrum of noise received by the hydrophone from the sources of noise with the spectrum from Fig. 4 (parameters as in Fig. 4).

3. Noise model functions and statistical parameters

The dependencies presented above describe the proposed surface noise model. We will further define its functions and statistical parameters, namely, the correlation functions, the Pearson correlation coefficients (Cohen, 1988), and the standard deviations of noise. We will calculate the correlation function in the frequency domain from the following formulas (Franks, 1981):

$$R_{12}(t) = \mathfrak{I}^{-1}\{\mathfrak{I}[N_1(f)] \cdot \mathfrak{I}^*[N_2(f)]\}$$
and
$$R_{56}(t) = \mathfrak{I}^{-1}\{\mathfrak{I}[N_5(f)] \cdot \mathfrak{I}^*[N_6(f)]\}, \tag{38}$$

where $N_i(f) = \mathfrak{I}\{n_{si}(t)\}$.

The parameters of the surface noise model are the radius of the circle R, on which the sources of noise are located, the surface density $\rho$of these sources, the variance of noise emitted and the distance of the real sources from the virtual sources $2a$. The noise correlation functions and correlation coefficient are also affected by the system parameters: antenna immersion depth h, hydrophone distance $2d$, filter band B, and sample rate f_s. We select the model parameters in such a manner that their properties are not sensitive to their changes in a relatively broad range. The constancy of the correlation coefficient as a function of the model parameters can be assumed as a criterion. It is evident that the greater the number of noise sources and the larger the radius of the surface containing these sources, the better the model corresponds to the reality. In view of the desired limitation of the numerical operations performed, the smallest acceptable R and ρ values should be sought. The tests carried out showed that stable results are obtained when $R/h \geq 10$ and the minimum surface density $\rho = 1/\mathrm{m}^2$. This density ensures a sufficient number of noise sources in the area near the Z-axis. A constant sample rate value $f_s = 300$ kHz is assumed to provide sufficient measurement time resolution for the smallest distance $d = 0.05$ m. It corresponds to 20 time samples.

In the calculations, we take into account the $y(k)$ coordinate of the noise sources for which the abovementioned dependencies have been omitted, as they do not differ from those provided for the $x(k)$ coordinate.

Figure 8 shows the correlation functions for a horizontal hydrophone pair, normalised by the maximum values, and Fig. 9 presents those functions for a vertical hydrophone pair. The graphs are made for noise with a constant noise power density. The width of the correlation function is larger with the narrower the B filter bandwidth. With wide B bandwidths, the correlation function is limited by the $\pm 2d/c$ times, marked with point lines. At a bandwidth of $B = 50$ kHz, there are

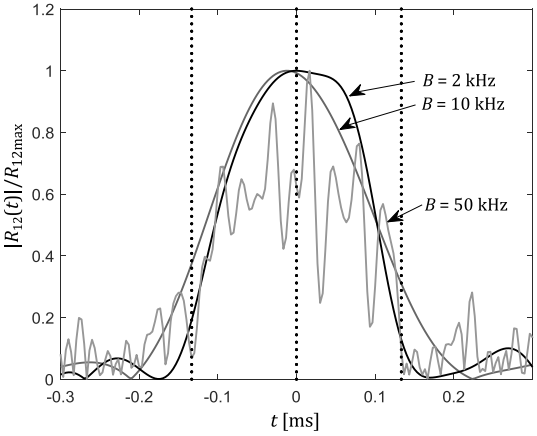

Fig. 8. Correlation function for the horizontal hydrophones ($R = 100$ m, $h = 10$ m, $\rho = 1/\mathrm{m}^2$, $d = 0.1$ m, $f_s = 300$ kHz, $T = 0.1$ s, $K \approx 31,400$).

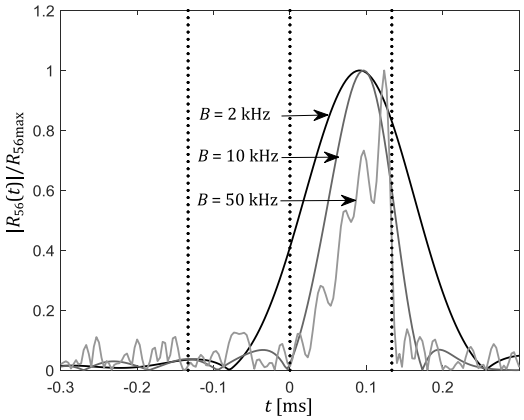

Fig. 9. Correlation function for the vertical hydrophones (parameters as in Fig. 8).

large fluctuations as a function course. This is because the acoustic wavelength $\lambda = c/B = 3$ cm at this frequency is smaller than the distance of the hydrophones $2d = 20$ cm. The noise spectrum then has a number of harmonics with opposite signs, resulting in the appearance of local minima. In theory, the $R_{12}(t)$ correlation function should be symmetrical. Deviations from this principle in numerical calculations are due to the lack of symmetry of the random surface distribution of noise sources despite their very large number ($K \approx 31,000$). The maxima of the $R_{56}(t)$ function for the vertical hydrophone pair, with the B bandwidth increase, approaches the $2d/c$ time, and at high frequencies, the main function section is within the $(0–2d/c)$ time interval.

The shift of the symmetry axis of the vertical correlation function of a pair of hydrophones, visible in Fig. 9, is caused by a shorter propagation time of the acoustic wave emitted by noise sources lying on the sea surface received by the upper hydrophone. This effect also occurs in the following figures for vertical pairs of hydrophones, it does not occur for horizontal pairs of hydrophones, and also for the isotropic noise field (Rudnicki *et al.*, 2020). Figures 10 and 11

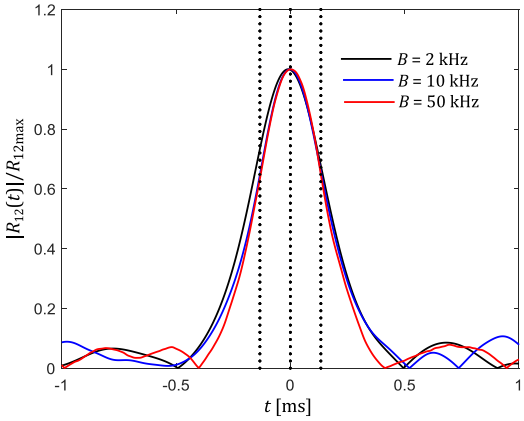

Fig. 10. Correlation function for the horizontal hydrophones (parameters as in Fig. 8).

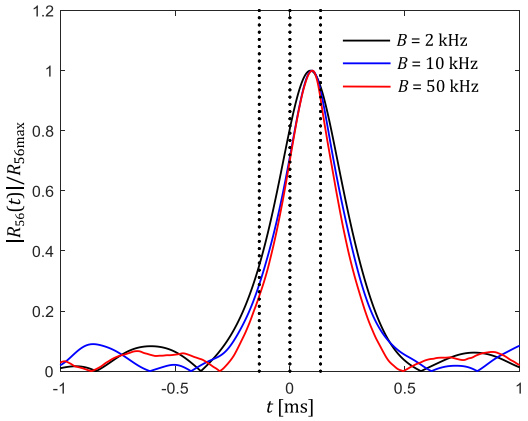

Fig. 11. Correlation function for the vertical hydrophones (parameters as in Fig. 8).

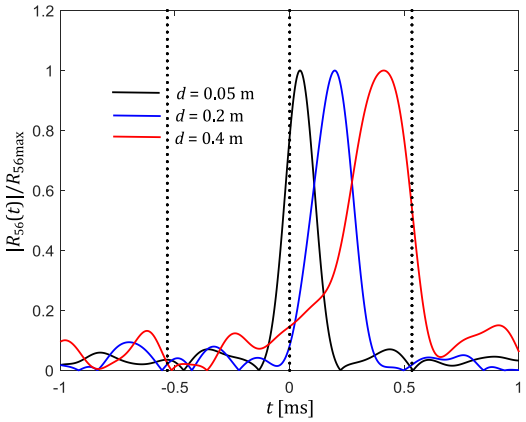

Fig. 13. Correlation function for the vertical hydrophones (parameters as in Fig. 12).

show correlation functions when the noise spectral density decreases at a rate of 6 dB/oct above a frequency of 500 Hz, as shown in Fig. 6. The course of the noise spectral density is similar to that of the function of a low-pass filter with an upper limit frequency of 500 Hz. As a result, the correlation function shapes are similar to those shown in Figs 8 and 9 for the bandwidth of a $B = 2$ kHz width. The effect of the B filter bandwidth is limited, as the filters only change the inclination of the function resulting from attenuation.

The course of the correlation function depends on the distance of the hydrophones, as shown in Figs 12 and 13, made for a frequency attenuation of 0 dB/oct. It is evident that the width of the correlation function is limited by the $2d/c$ frequencies. In the figures, these limits are marked for $d = 0.4$ m. The cause of the fluctuation of the correlation function is the same as that discussed for Figs 8 and 9. At a frequency of 2 kHz, the wavelength is 0.75 m and is smaller than $2d = 0.8$ m. In general, there is no reason for any fluctuation when half the wavelength for the high frequency of the noise spectrum is greater than the distance of the hydrophones.

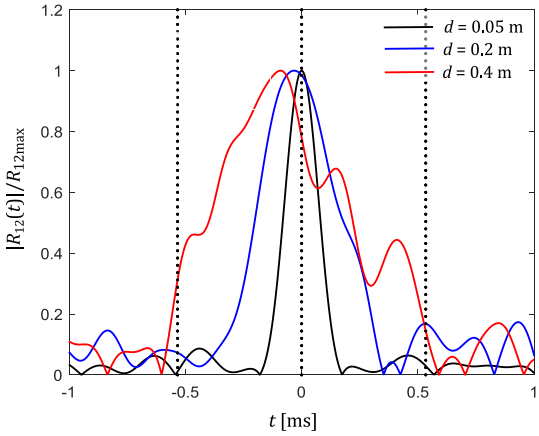

Fig. 12. Correlation function for the horizontal hydrophones ($R = 100$ m, $h = 10$ m, $\rho = 1/\mathrm{m}^2$, $B = 2$ kHz, $f_s = 300$ kHz, $K \approx 31,400$).

The fact that the correlation function is not affected by the h antenna immersion depth is illustrated in Figs 14 and 15. The graphs were made for a constant number of noise sources and a surface radius of $R = 10h$, modifying the surface density of the noise sources accordingly. This is due to the limited memory

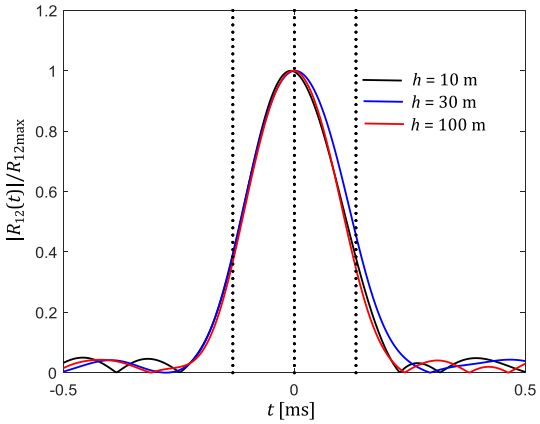

Fig. 14. Correlation function for the horizontal hydrophones ($d = 0.1$ m, $B = 2$ kHz, $f_s = 300$ kHz, $T = 0.1$ s, $K \approx 31,400$).

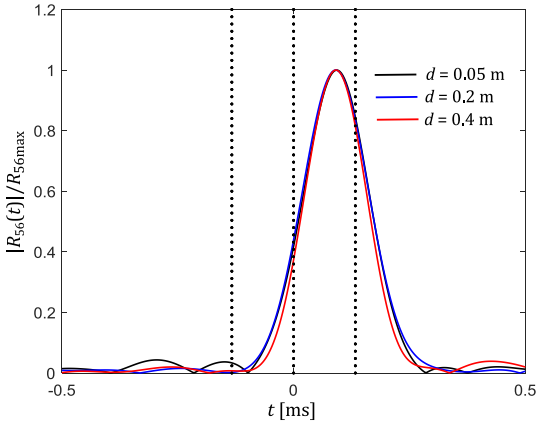

Fig. 15. Correlation function for the vertical hydrophones (parameters as in Fig. 12).

of the MATLAB® environment, as at a constant density, the number of K sources grows with the square of the R radius reaching more than 3 million for $h = 100$. This has no significant impact on the quality of the results, as with the increase of the depth, the number of sources in a constant solid angle around the Z-coordinate increases.

The effect of the B bandwidth of the low-band filter on the noise model parameters is shown in Figs 16 and 17. The parameters are normalised by the corresponding parameter at a bandwidth of $B = 1$ kHz. The values of these parameters are given under the figure captions. They do not have physical values, but they are used to compare the parameters of horizontal and vertical hydrophone pairs. With an increase in the B bandwidth of the filter, there is an increase in the standard noise deviation σ. This is because, with a constant noise spectral density, the power of the noise received increases in proportion to the bandwidth of the noise. As the B bandwidth increases, the noise correlation is reduced, as shown in the graph of the r_{12} and r_{56} correlation coefficients.

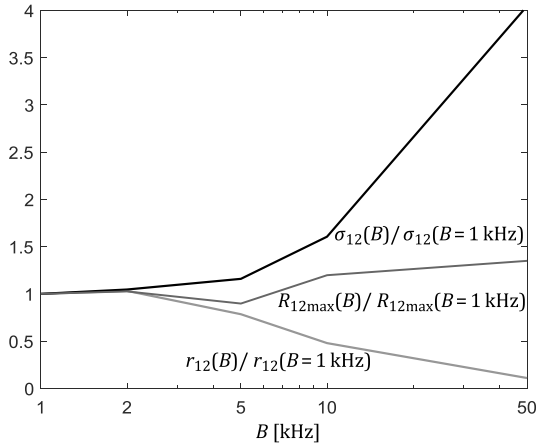

Fig. 16. Model parameters for the horizontal hydrophone pair; $B_1 = 1$ kHz, $\sigma_{12}(B_1) = 0.025$, $r_{12}(B_1) = 0.03$, $R_{12\,\text{max}}(B_1) = 142$ ($d = 0.1$ m, $h = 10$ m, $R = 100$ m, $f_s = 300$ kHz, $T = 0.1$ s, $K \approx 31,400$).

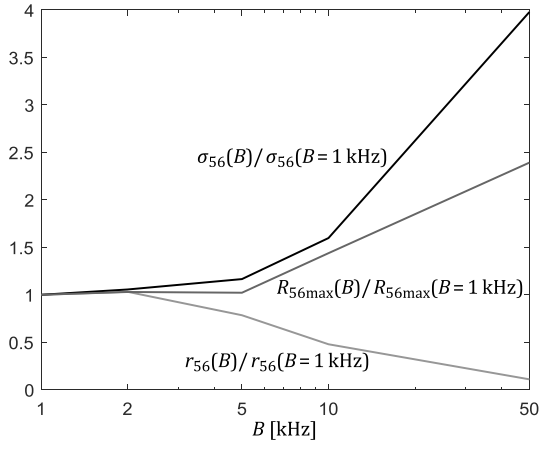

Fig. 17. Model parameters for the vertical hydrophone pair; $B_1 = 1$ kHz, $\sigma_{56}(B_1) = 0.025$, $r_{56}(B_1) = 0.37$, $R_{56\,\text{max}}(B_1) = 195$ (parameters as in Fig. 16).

Figure 17 shows the $R_{56\,\text{max}}$ correlation function maximum increase with the increase in B bandwidth, which is related to the movement of the maximum of this function in the direction of the $2d/c$ time and its near-triangle shape (Buckingham, 2012; Barclay, Buckingham, 2014; Cron, Sherman, 1962; 1965).

Figures 18 and 19 show the effect of hydrophone distance d on the model parameters. The standard deviation of the noise received is constant as it applies to a single hydrophone. As the hydrophone distance increases, the level of noise correlation is reduced, as can be seen from the graphs of the r_{12} and r_{56} correlation coefficients and the maximum values of the correlation function $R_{12\,\text{max}}$ and $R_{56\,\text{max}}$. It is because the delays between the noise received by the hydrophone pairs are increasing. The graphs are normalised by the parameters for $d = 0.05$ m.

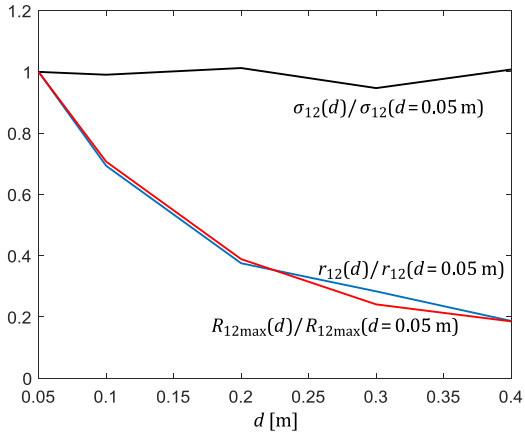

Fig. 18. Model parameters for the horizontal hydrophone pair, $d_1 = 0.05$ m, $\sigma_{12}(d_1) = 0.025$, $r_{12}(d_1) = 0.87$, $R_{12\,\text{max}}(d_1) = 184$ (parameters as in Fig. 16).

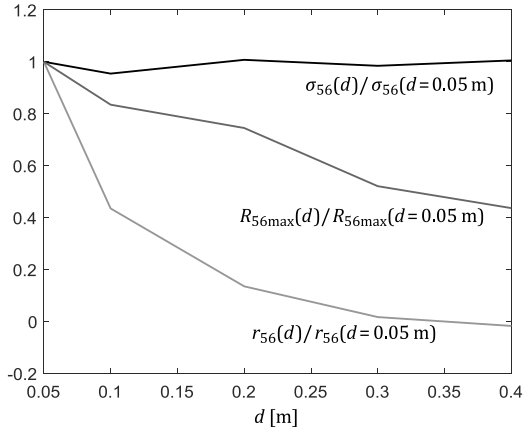

Fig. 19. Model parameters for the vertical hydrophone pair; $d_1 = 0.05$ m, $\sigma_{56}(d_1) = 0.025$, $r_{56}(d_1) = 0.76$, $R_{56\,\text{max}}(d_1) = 205$ (parameters as in Fig. 16).

The results of the calculation of the impact of the h antenna immersion depth on the model parameters

showed no such relationship in the range between 10 m and 100 m; the parameters are fixed. The calculation assumes a constant noise source surface density of ρ and increases the R radius of the noise circle in proportion to the h antenna immersion depth: $R = 10h$. As the h immersion depth increased, the number of active noise sources increased, which compensated for the increase in transmission losses. This also results from formula (9) in which the value of noise received is proportional to the h immersion depth.

At the end, Figs 20 and 21 show the correlation functions for 0 dB/oct attenuation without noise filtering. The noise bandwidth is limited by the sampling rate. The correlation function shapes are similar to those obtained theoretically (Buckingham, 2012; Barclay, Buckingham, 2014; Cron, Sherman, 1962; 1965).

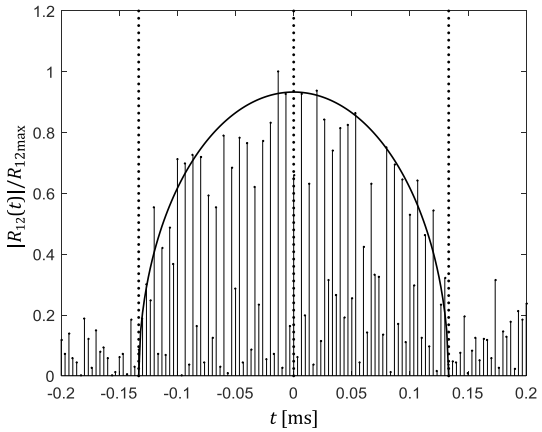

Fig. 20. Correlation function for the horizontal hydrophones, $B = f_s/2$ (parameters as in Fig. 16).

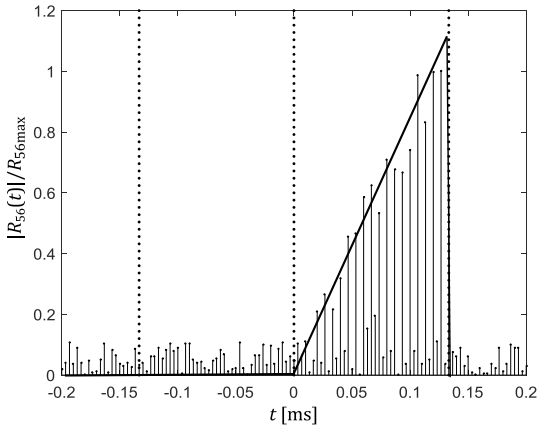

Fig. 21. Correlation function for the vertical hydrophones, $B = f_s/2$ (parameters as in Fig. 20).

4. Application of the noise model in a DIFAR-type system analysis

Radio direction finding systems used before World War II to determine the bearing of radio transmitters served as the prototype of the currently used DIFAR-type systems (Jagodziński, 1961). As a result of the current digital signal processing capabilities, the historical solutions have been complemented by online Fourier transforms, which significantly improves the system's performance. The current design and operating principle of the DIFAR system is discussed in detail in (Rudnicki *et al.*, 2020) and here we will only show the subsequent stages of signal processing in simulation tests.

Let us assume that the signal source is very far away from the antenna and, as a result, delays in receiving signals only depend on the source bearing. These signals can therefore be expressed as:

$$s_i(t) = s_0 s(t - \tau_i), \tag{39}$$

where i is the hydrophone number shown in Fig. 1, s_0 is the amplitude of the received signals, and τ_i is the delay in the i-th hydrophone in relation to the centre of the coordinate system. If you mark the azimuth angle with φ and the elevation angle with θ, these delays are equal to:

$$\begin{aligned} \tau_1 &= -\frac{d}{c}\sin\theta\cos\varphi, & \tau_2 &= \frac{d}{c}\sin\theta\cos\varphi, \\ \tau_3 &= -\frac{d}{c}\sin\theta\cos\varphi < & \tau_4 &= \frac{d}{c}\sin\theta\cos\varphi, \\ \tau_5 &= -\frac{d}{c}\sin\theta\cos\varphi, & \tau_6 &= \frac{d}{c}\sin\theta\cos\varphi. \end{aligned} \tag{40}$$

The signals received are summed with the noise generated by their numerical model described above and then subtracted in pairs. The result is:

$$x(t) = [s_1(t) + n_{s1}(t)] - [s_2(t) + n_{s2}(t)], \tag{41}$$

$$y(t) = [s_3(t) + n_{s3}(t)] - [s_3(t) + n_{s3}(t)], \tag{42}$$

$$z(t) = [s_5(t) + n_{s5}(t)] - [s_6(t) + n_{s6}(t)], \tag{43}$$

where $n_{si}(t)$ is described by formula (37).

The signals described with the above dependencies are optionally filtered in finite impulse response filters, which, as known, have linear phase characteristics (Salamon, 2006; Lyons, 2004) and then undergo the Fourier transform. At the same time, the Fourier transform of the signal received by the central hydrophone $u(t) = s(t) + n(t)$ is calculated. When marking the $u(t)$ transform as $U(f)$, the following operations are performed:

$$X(f) = \text{imag}\,[\Im\{x(t)\} \cdot U^*(f)], \tag{44}$$

$$Y(f) = \text{imag}\,[\Im\{y(t)\} \cdot U^*(f)], \tag{45}$$

$$Z(f) = \text{imag}\,[\Im\{z(t)\} \cdot U^*(f)], \tag{46}$$

where * denotes the conjugate function.

For each spectrum lines, the azimuth angle φ of the real or virtual source (resulting from the existence of noise) shall be calculated using the dependency:

$$\varphi = \arctan\left(\frac{X(f)}{Y(f)}\right), \tag{47}$$

and the θ elevation angle from the formula:

$$\theta = \arcsin\left(\frac{Z(f)}{\sqrt{X^2(f)+Y^2(f)}}\right). \tag{48}$$

With a good signal-to-noise ratio, the maxima of the $X(f)$, $Y(f)$, and $Z(f)$ spectra occur at the sine-signal frequency and for this frequency we obtain the source bearings sought, as shown in (Rudnicki *et al.*, 2020). The presence of noise results in errors in the determination of bearings.

Examples of simulation results described with the above formulas are shown in Figs 22 and 23. The points in Fig. 22 have Cartesian coordinates $X(f)$ and $Y(f)$ for each frequency f. The slope of the lines connecting these points to the centre of the coordinate system describes the measured azimuth. Similarly, the points in Fig. 23 have coordinates on the X axis with the vector length $[X(f), Y(f)]$, ref. formula (48), and on the Y-axis with the length $Z(f)$. The results of 10 measuring cycles in the range of a bandwidth of B of the filter are presented. The caption of Fig. 22 defines the surface noise model parameters and system parameters. The average value of the azimuth error is $-0.5°$ and its standard deviation is $1.9°$. Elevation errors are $0.9°$ and $3.7°$, respectively. The central part of the figure shows the azimuth and elevation measurements related to noise.

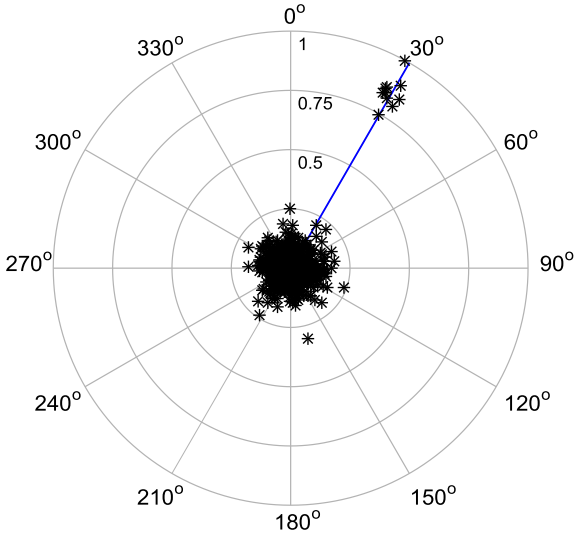

Fig. 22. Azimuth measurement results (R = 100 m, h = 10 m, $\rho = 1/\mathrm{m}^2$; $K \approx 31,400$; d = 0.1 m, f_s = 300 kHz, B = 2 kHz, T = 0.1 s, SNR_i = −8 dB).

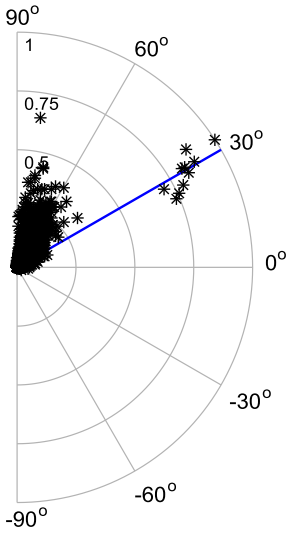

Fig. 23. Elevation measurement results (parameters as in Fig. 22).

The input signal-to-noise ratio is defined as:

$$\mathrm{SNR}_i = 10\log\frac{s_0^2}{2\sigma_f^2}, \tag{49}$$

where s_0 is the amplitude of the sine signal, and σ_f^2 is the variance of noise at the filter output.

From the point of view of the system operation, two of its parameters are important, namely, the magnitude of bearing errors and the output signal-to-noise ratio (SNR_o), which determines its detection capabilities and bearing errors. We will investigate further whether these parameters depend on the levels of environmental noise and how closely they are correlated. The output signal-to-noise ratio is calculated using the following dependency:

$$\mathrm{SNR}_o = 10\log\frac{A_{\max}^2}{A^2(f)}. \tag{50}$$

For the azimuth, $A_{\max}^2$ is the maximum value of the function $[X^2(f) + Y^2(f)]$ and for the elevation of the function $[X^2(f) + Y^2(f) + Z^2(f)]$. The expression in the denominator describes the variance of the noise spectrum calculated using the above formulas, excluding the maximum value associated with the sine signal.

A very large measurement error occurs when the $A_{\max}$ maximum value does not apply to the signal but is associated with noise. The probability of this event increases as the quotient of the $A_{\max}$ maximum value of signal $A_{\max n}$ maximum value of noise decreases. This quotient is expressed logarithmically as $\mathrm{SNR}_n = 20\log(A_{\max}/A_{\max_n})$. Figure 24 shows the relationship between both signal-to-noise ratios and the SNR_i input signal-to-noise ratio.

The figure shows a worse output signal-to-noise ratio when measuring elevation, which can also be seen

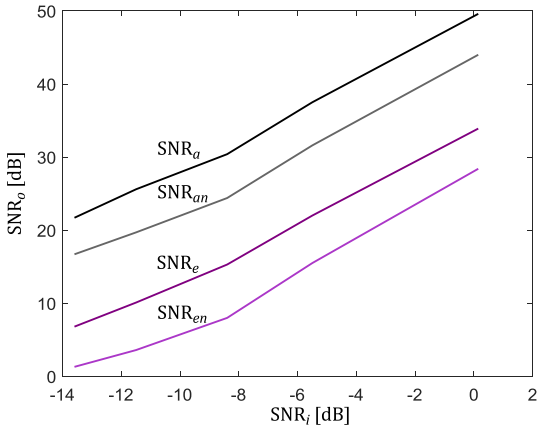

Fig. 24. Dependency of the output signal-to-noise ratio (SNR$_a$ – of the azimuth, SNR$_e$ – of the elevation) and the input signal-to-noise ratio ($R = 100$ m, $h = 10$ m, $\rho = 1/\mathrm{m}^2$; $K \approx 31,400$, $d = 0.1$ m, $f_s = 300$ kHz, $f_0 = 50$ Hz, $B = 2$, $T = 0.1$ s).

in Fig. 23. This is related to a greater impact of noise sources located on the sea surface on the vertical hydrophone pair. Above all, there is a significant improvement in the output signal-to-noise ratio relative to the input ratio. In addition, this improvement increases as the input signal-to-noise ratio increases, which is untypical. For example, in active systems, usually there is $\mathrm{SNR}_o = D + \mathrm{SNR}_i$, where D is the so called conversion gain. Figure 24 shows that in the case at hand there is approximately: $\mathrm{SNR}_o \approx D + 2\mathrm{SNR}_i$. This is due to the dependencies (44)–(46) in which the spectra are multiplied by the $U(f)$ spectrum, which is the sum of the signal spectrum and the noise spectrum. In active systems with matched filtration (correlation reception), the spectrum of the received signal is multiplied by the spectrum of the known undistorted scanning signal (Salamon, 2006).

Figure 25 shows that the bearing errors decrease as the input signal-to-noise ratio increases, starting with a definite small value of that ratio. In the case

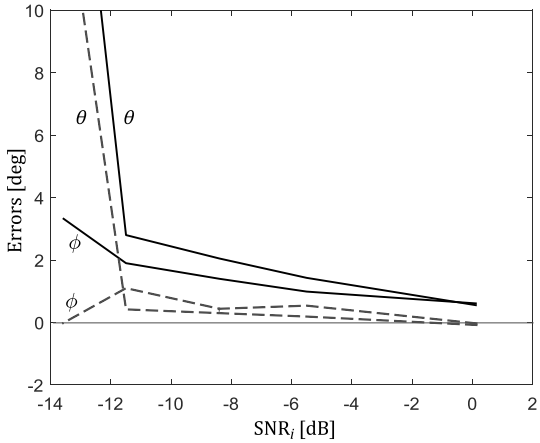

Fig. 25. Bearing errors as a function of the input signal-to-noise ratio (parameters as in Fig. 24).

presented in the figure, this value is $\mathrm{SNR}_i \approx -11$ dB. This is because of the bearing error method, which calculates errors against the $A_{\max}$ maximum value. As stated above, with a low signal-to-noise ratio, the maximum values associated with noise may be greater than the signal values, as shown in Figs 26 and 27, referring to the results presented in Fig. 25 for $\mathrm{SNR}_i = -13$ dB. However, it should be noted that in the practical operation of the system, it is possible to estimate bearings with a lower signal-to-noise ratio, since the results of measurements in subsequent transmissions relating to the signal are arranged along regular lines and the noise-related results are distributed randomly. This is shown in Fig. 27.

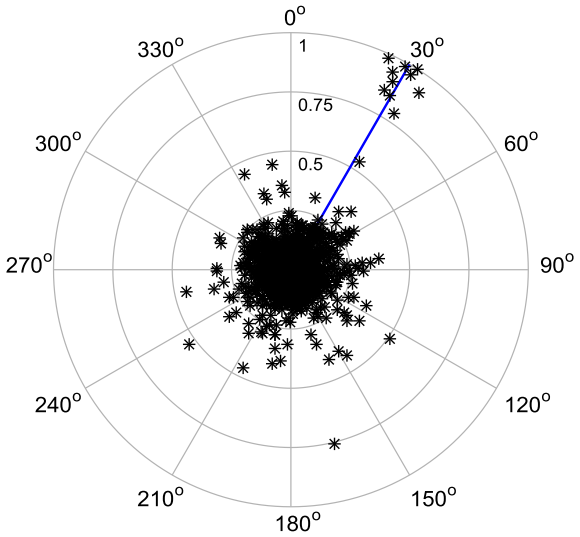

Fig. 26. Azimuth measurement results; $\mathrm{SNR}_i = -13$ dB (parameters as in Fig. 24).

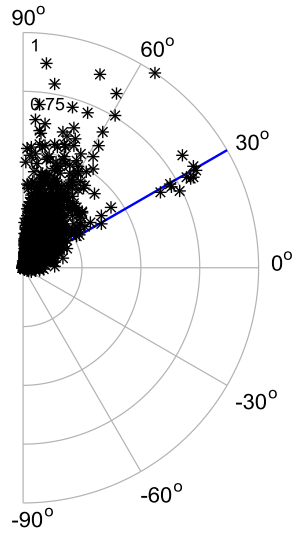

Fig. 27. Elevation measurement results; $\mathrm{SNR}_i = -13$ dB (parameters as in Fig. 24).

In addition to the impact of the input signal-to-noise ratio on bearing errors, it can be expected that they are affected by the level of noise correlation. The

value of the correlation coefficients depends on, i.a., the bandwidth B, assuming a constant noise spectral density of the medium noises. The results of the calculations are shown in Table 1. The σ^2 symbol denotes the variance of noise at the hydrophone output after filtration, the σ_{12}^2 symbol denotes the variance of the difference of noise in the H_1 and H_2 hydrophone pairs, and σ_{12t}^2 is the theoretical value of this variance calculated using the formula $\sigma_{12t}^2 = 2\sigma^2(1-r_{12})$. The $\overline{\varphi}$ symbol denotes the average azimuth error calculated based on ten transmissions and σ_φ is the standard deviation of this error. The same symbols apply for elevation errors.

Table 1. Bearing errors as a function of noise bandwidth (parameters as in Fig. 24).

	B [kHz]				
	1	2	2	4	5
SNR_i [dB]	−2.0	−4.9	−6.9	−8.3	−9.2
r_{12}	0.97	0.87	0.79	0.63	0.49
r_{56}	0.94	0.75	0.54	0.34	0.13
σ^2	0.59	1.58	2.37	3.33	4.30
σ_{12}^2	0.037	0.41	1.02	2.51	4.20
σ_{12t}^2	0.037	0.41	1.03	2.52	4.21
$\overline{\varphi}$ [deg]	0.02	0.02	0.28	0.04	0.57
σ_φ [deg]	0.98	1.52	1.35	1.34	1.49
$\overline{\theta}$ [deg]	−0.64	−0.41	1.42	0.15	−0.97
σ_θ [deg]	1.60	1.49	1.56	1.71	1.98

The results presented in the table above show no significant correlation between bearing errors and the noise bandwidth B and the SNR_i input signal-to-noise ratio resulting from variations in noise bandwidth. An increase in noise bandwidth causes a decrease of the r_{12} and r_{56} correlation coefficients, which also suggests that the bearing errors are not dependent on the level of noise correlation. This dependency does not occur despite the increase in the σ^2 variance of noise at the hydrophone output after filtration and a more prominent change in the σ_{12}^2 variance of the difference of noise received by the hydrophone pair. This variance does not differ from its theoretical value of σ_{12t}^2 calculated using the above formula.

The calculations made also showed that the $2d$ distance of hydrophone pairs does not affect the bearing errors, as it is also shown in (Rudnicki *et al.*, 2020). This work provides a general explanation of the absence of the relationship discussed. However, its full justification goes beyond the framework of this article, as it requires a complex theoretical analysis of the errors resulting from the formulas (44)–(48). It should be stressed that the hypothesis that noise correlation has no effect on bearing errors is false and results from the use of a popular description of correlations with correlation functions and correlation coefficients relating to the time domain. However, the system operates in the frequency domain.

The hypothesis of no correlation of bearing errors is undermined by the calculation results shown in Fig. 28 made for the uncorrelated noise model. This model assumes that noise emitted by individual sources is received by the hydrophones as uncorrelated. For comparison, bearing errors were determined for the same parameters as in Fig. 25, relating to the correlated noise model.

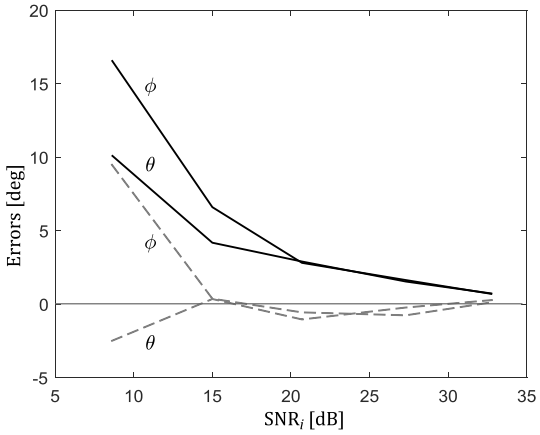

Fig. 28. Bearing errors for uncorrelated noise as a function of the input signal-to-noise ratio (parameters as in Fig. 24).

When comparing the figure above with Fig. 25, we can see that the bearing errors of similar values occur for uncorrelated noise with an input signal-to-noise ratio of approximately 30 dB higher than for correlated noise. This fact should be taken into account when designing DIFAR-type systems.

Figures 29 and 30 show azimuth measurements corresponding to the two input signal-to-noise ratios in Fig. 28.

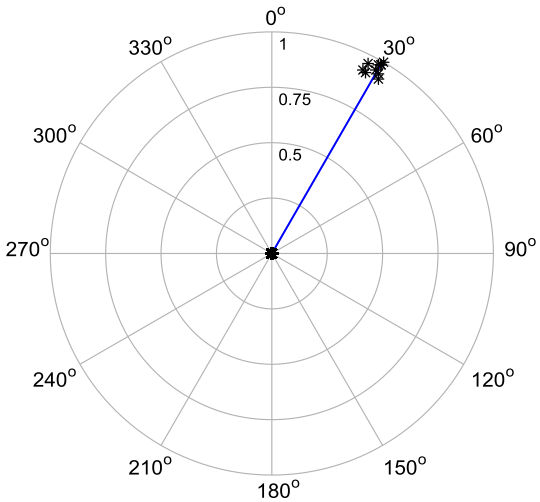

Fig. 29. Azimuth measurement results for uncorrelated noise, $SNR_i \approx 30$ dB (parameters as in Fig. 24).

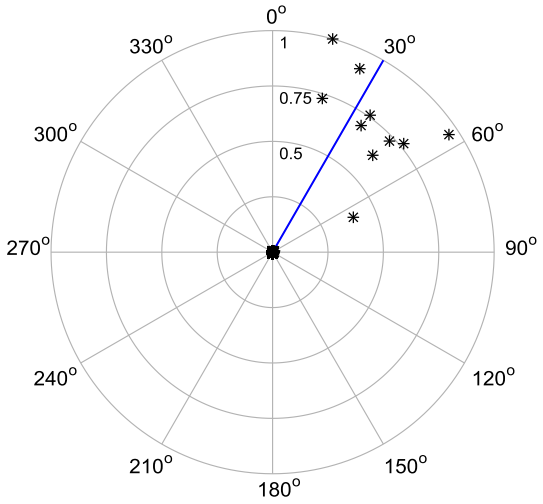

Fig. 30. Azimuth measurement results for uncorrelated noise, $SNR_i \approx 10$ dB (parameters as in Fig. 24).

The above figures show that the output signal-to-noise ratio is in both cases large, as evidenced by a spot with a small diameter in the centre of the coordinate system. Unlike the model of correlated noise, large bearing errors do not occur as a result of the appearance of maximum $A_{\max}$ lines coming from noise, but result only from the decreasing input signal-to-noise ratio.

5. Conclusions

The numerical sea wave noise model presented in the article is consistent with the results of theoretical works and measurements at sea (Buckingham, 2012; Barclay, Buckingham, 2014; Cron, Sherman, 1962; 1965). It can therefore be used during the design phase of systems of the DIFAR type and other passive underwater acoustics systems. This is evidenced by the demonstrated examples of the DIFAR system simulations. A full explanation of the relationship of bearing errors with noise correlation requires an in depth analysis, the results of which the authors intend to include in a separate publication.

The consequence of introducing a noise-emitting surface in the model is to limit the sphere containing noise sources in the previously adopted model by the plane of the sea surface (Rudnicki *et al.*, 2020). By summing the noise generated by sources located on the sea surface and the noise emitted by sources in the truncated sphere in appropriate proportions, a combined noise model that better reflects the noise field in real bodies of water can be developed (publication under preparation).

References

1. Barclay D.R., Buckingham M.J. (2014), On the spatial properties of ambient noise in the Tonga Trench, including effects of bathymetric shadowing, *The Journal of the Acoustical Society of America*, **136**(5): 2497–2511, doi: 10.1121/1.4896742.
2. Buckingham M.J. (2012), Cross-correlation in band-limited ocean ambient noise fields, *The Journal of the Acoustical Society of America*, **131**(4): 2643–2657, doi: 10.1121/1.3688506.
3. Burdick W.S. (1984), *Underwater Acoustic System Analysis*, Prentice-Hall, Englewood Cliffs, NJ.
4. Cohen J. (1988), *Statistical Power Analysis for the Behavioral Sciences*, 2nd ed., Lawrence Erlbaum Associates, Publishers.
5. Crocker M.J. (1998), *Handbook of Acoustics*, John Wiley & Sons.
6. Cron B.F., Sherman C.H. (1962), Spatial-correlation functions for various noise models, *The Journal of the Acoustical Society of America*, **34**(11): 1732–1736, doi: 10.1121/1.1909110.
7. Cron B.F., Sherman C.H. (1965), Addendum: Spatial correlation functions for various noise models [*J. Acoust. Soc. Am.*, **34**: 1732–1736 (1962)], *The Journal of the Acoustical Society of America*, **38**(4): 885, doi: 10.1121/1.1909826.
8. Franks L.E. (1981), *Signal Theory. Revised Edition*, Dowden & Culver, Inc.: Stroudsburg, PA.
9. Grelowska G., Kozaczka E., Kozaczka S., Szymczak W. (2013), Underwater noise generated by small ships in the shallow sea, *Archives of Acoustics*, **38**(3): 351–356, doi: 10.2478/aoa-2013-0041.
10. Jagodziński Z. (1961), *Radionavigation Systems* [in Polish], Wydawnictwo MON, Warszawa.
11. Klusek Z., Lisimenka A. (2004), Characteristics of underwater noise generated by single breaking wave, *Hydroacoustics*, **7**: 107–114.
12. Klusek Z., Lisimenka A. (2016), Seasonal and diel variability of the underwater noise in the Baltic Sea, *The Journal of the Acoustical Society of America*, **139**(4): 1537–1547, doi: 10.1121/1.4944875.
13. Kochańska I., Nissen I., Marszal J. (2018), A method for testing the wide-sense stationary uncorrelated scattering assumption fulfillment for an underwater acoustic channel, *The Journal of the Acoustical Society of America*, **143**(2): EL116–EL120, doi: 10.1121/1.5023834.
14. Kozaczka E., Grelowska G. (2011), Shipping low frequency noise and its propagation in shallow water, *Acta Physica Polonica A*, **119**(6A): 1009–1012, doi: 10.12693/APhysPolA.119.1009.
15. Lyons R.G. (2004), *Understanding Digital Signal Processing*, 2nd ed., Prentice Hall, Inc.
16. Mallet A.L. (1975), *Underwater Direction Signal Processing System*, US Patent No 3,870,989.

17. Ren C., Huang Y. (2020), A spatial correlation model for broadband surface noise, *The Journal of the Acoustical Society of America*, **147**(2): EL99–EL105, doi: 10.1121/10.0000710.

18. Rudnicki M., Marszal J., Salamon R. (2020), Impact of spatial noise correlation on bearing accuracy in DIFAR systems, *Archives of Acoustics*, **45**(4): 709–720, doi: 10.24425/aoa.2020.135277.

19. Salamon R. (2006), *Sonar systems* [in Polish], Gdańskie Towarzystwo Naukowe, Gdańsk, Poland.

20. Schmidt J.H., Schmidt A., Kochańska I. (2018), Multiple-Input Multiple-Output Technique for Underwater Acoustic Communication System, [In:] *Proceedings of 2018 Joint Conference – Acoustics, Ustka, Poland, 2018, IEEE Xplore Digital Library*, pp. 280–283, doi: 10.1109/acoustics.2018.8502439.

21. Urick R.J. (1983), *Principles of Underwater Sound*, 3rd ed., Peninsula Pub.

22. Urick R.J. (1986), *Ambient Noise in the Sea*, 2nd ed., Peninsula Pub.